Peer-Reviewed Technical Communication

Source Localization With Multiple Hydrophone Arrays via Matched-Field Processing

Dag Tollefsen and Stan E. Dosso

Abstract—This paper considers approaches to combining information from multiple arrays in matched-field processing (MFP) for underwater acoustic source localization. The standard approach is to apply conventional MFP for each array independently, and sum the resulting Bartlett ambiguity surfaces computed for each array; this approach assumes that individual arrays comprise calibrated sensors which are synchronized in time. However, if the relative calibration and/or time synchronization is known between some or all arrays, more informative multiple-array processors can be derived using maximum-likelihood methods. If the relative calibration between arrays is known, the observed variation in received signal amplitude between arrays provides additional information for matched-field localization which is absent in the standard processor. If synchronization is known between arrays, phase variations provide additional localization information. Multiple-array processors accounting for different levels of interarray information are derived and evaluated in terms of the probability of correct localization from Monte Carlo analyses for a range of signal-to-noise ratios and the number of frequencies for simulated shallow-water scenarios with multiple horizontal and/or vertical arrays. The analysis indicates that, dependent on array configurations, significant improvements in source localization performance can be achieved when including relative amplitude and/or phase information in the multiple-array processor. The improvement is reduced by environmental and array (calibration and synchronization) mismatch; however, this degradation can be partially mitigated by including additional frequencies in the processing.

Index Terms—Acoustic array systems and processing, matched-field processing (MFP) in underwater acoustics, passive sonar systems.

I. INTRODUCTION

THE use of acoustic hydrophone arrays for 2-D and 3-D source localization in shallow water has received considerable interest for application to localization of ships and sources [1]–[9] and for passive acoustic monitoring of marine mammals [10]–[16]. For long-duration signals, such as harmonic noise from ships, estimation of source bearing with a horizontal line array (HLA) is typically accomplished by beamforming

(the pressure field time series received at an acoustic array is correlated with a model plane-wave signal due to a far-field source from a given look direction); source range can then be estimated via triangulation using bearing estimates from multiple arrays [17]. For transient signals, e.g., short-duration clicks from marine mammals, alternative methods for bearing estimation have been developed based on estimated time differences of arrival (TDOA) at two or more sensors of an array [11]–[15]. By incorporation of acoustic-path considerations or numerical acoustic propagation models in processing, TDOA methods have been extended to include source depth estimation, range estimation, and 3-D source localization [11]–[14]. For applications to ships and moving sources, matched-field processing (MFP) [2]–[8] is a widely used source localization method. MFP is based on matching the acoustic pressure field measured at an array of sensors with modeled replica fields computed for the acoustic waveguide via a numerical propagation model over a grid of possible source positions, with the position estimate taken to be the grid point of maximum match.

Recent applications in passive acoustic monitoring include the combination of source location estimates from short-aperture arrays, distributed single-hydrophone sensors, and combinations of an array and single sensors [12]–[16]. These applications carry out localization estimation for each sensor or array individually, then combine results in a subsequent step. Hence, processor values, but not acoustic data, are combined between multiple arrays; this is in contrast to the approach in this paper, where new MFP processors are developed which combine acoustic data across arrays. While many aspects of MFP performance have been studied theoretically and with simulations and measured data, there appears to have been little work on MFP performance for multiple, spatially separated arrays. One approach is given in [5], where adaptive MFP was applied to data from three vertical line arrays (VLAs) in shallow water, with interarray phase and amplitude differences precomputed based on auxiliary nonacoustic source track information and known array geometries.

This paper considers matched-field localization for application to processing data from multiple acoustic arrays. The sensors within each individual array are assumed to be calibrated and time synchronized to allow for conventional phase-coherent MFP over the spatial extent (aperture) of that array. Multiple-array processing can, in general, include cases with interarray

information on relative amplitude (when knowledge of the relative calibration of arrays is available) and/or relative phase (for arrays which are synchronized with each other in time). In the approach developed in this paper, the unknown complex source strength (source amplitude and phase at each frequency) and source position are estimated by combining information from multiple arrays in an optimal manner as derived using maximum-likelihood (ML) methods. The processors derived are applicable to general combinations of array configurations; here they are applied to simulated data for HLAs and/or VLAs in a simulated shallow-water scenario. Processor performance is evaluated in terms of the probability of correct localization (PCL) from Monte Carlo analysis for a range of signal-to-noise ratios (SNRs) and a number of frequencies. Effects of environmental mismatch [18] due to uncertainties in water depth and seabed geoacoustic parameters, and effects of mismatch due to errors in array calibration or synchronization are also addressed, and the ability to (partially) compensate for mismatch effects by using larger numbers of frequencies is considered.

II. MULTIPLE-ARRAY MAXIMUM-LIKELIHOOD PROCESSORS

ML processors for multiple arrays can be derived by maximizing the likelihood function analytically over unknown source parameters for various assumptions on relative amplitude and phase information between the arrays. Under the assumption of complex, circularly symmetric Gaussian-distributed errors, which are independent between arrays and frequencies, the likelihood function for source position $\mathbf{x}$ is given by

$$L(\mathbf{x}) = \prod_{f=1}^{F} \prod_{j=1}^{J} \frac{1}{\left(\pi \sigma_{fj}^2\right)^{N_j}} \exp\left[-\left|\mathbf{d}_{fj} - S_{fj}\hat{\mathbf{d}}_{fj}(\mathbf{x})\right|^2 / \sigma_{fj}^2\right]$$

$$\propto \exp\left[-\sum_{f=1}^{F} \sum_{j=1}^{J} \left|\mathbf{d}_{fj} - S_{fj}\hat{\mathbf{d}}_{fj}(\mathbf{x})\right|^2 / \sigma_{fj}^2\right] \quad (1)$$

where $\{\mathbf{d}_{fj}; f = 1, F; j = 1, J\}$ are the complex acoustic data at F frequencies and J sensor arrays, N_j is the number of hydrophones in array j, $\hat{\mathbf{d}}_{fj}(\mathbf{x})$ are the replica (modeled) acoustic fields due to a unit-amplitude, zero-phase source at location $\mathbf{x}$, S_{fj} is the unknown complex source strength (amplitude and phase) at the fth frequency as sensed by the jth array (i.e., S_{fj} is dependent on the calibration of array j), and σ_{fj} are the noise standard deviations (variances σ_{fj}^2). The ML processors can be derived based on the misfit or negative log-likelihood function [19], [20]

$$E(\mathbf{x}) = \sum_{f=1}^{F} \sum_{j=1}^{J} \left|\mathbf{d}_{fj} - S_{fj}\hat{\mathbf{d}}_{fj}(\mathbf{x})\right|^2 / \sigma_{fj}^2 . \quad (2)$$

Specific processors are derived based on various assumptions on relative source/array spectral information. For processors considered in the following, the source spectrum, i.e., relative source amplitude and/or phase as a function of frequencies, is assumed unknown. Three cases of relative spectral information between spatially separated arrays are examined in this paper. First, with no relative spectral information available between arrays (i.e., relative array calibrations unknown and arrays not synchronized with each other in time), the appropriate source term is $S_{fj} = A_{fj}e^{i\theta_{fj}}$ (amplitude A_{fj} and phase θ_{fj} are

unknown over both frequency and array). Maximizing the likelihood by setting $\partial E/\partial A_{fj} = 0$ and $\partial E/\partial \theta_{fj} = 0$ leads to ML amplitude and phase estimates

$$A_{fj} = \frac{\left|\mathbf{d}_{fj}^\dagger \hat{\mathbf{d}}_{fj}(\mathbf{x})\right|}{\left|\hat{\mathbf{d}}_{fj}(\mathbf{x})\right|^2} , \quad e^{i\theta_{fj}} = \left[\frac{\hat{\mathbf{d}}_{fj}^\dagger(\mathbf{x})\mathbf{d}_{fj}}{\mathbf{d}_{fj}^\dagger \hat{\mathbf{d}}_{fj}(\mathbf{x})}\right]^{1/2} \quad (3)$$

where † is the conjugate transpose. Substituting these expressions back into (2) leads to the ML processor for unknown interarray amplitude and phase (in the following termed the *incoherent multiple-array processor*, denoted E_{uu})

$$E_{\mathrm{uu}} = \sum_{f=1}^{F} \sum_{j=1}^{J} \frac{1}{\sigma_{fj}^2} \left\{|\mathbf{d}_{fj}|^2 - \frac{\left|\mathbf{d}_{fj}^\dagger \hat{\mathbf{d}}_{fj}(\mathbf{x})\right|^2}{\left|\hat{\mathbf{d}}_{fj}(\mathbf{x})\right|^2}\right\} . \quad (4)$$

This processor is recognized as an incoherent sum (over frequencies and arrays) of Bartlett mismatch processors weighted according to the variance at each frequency and array. Note that for this case, with the relative amplitude unknown between arrays, each correlation term is normalized by the replica magnitude at the array before summation over arrays; this removes information on the relative magnitude of fields at the various arrays which cannot be used if relative array calibrations are unknown.

The second case considered is where the relative amplitude and the relative phase spectra are both known between arrays (i.e., relative array calibrations are known and all arrays are synchronized with each other in time). The unknown source term can then be simplified to $S_{fj} = A_f e^{i\theta_f}$ (i.e., no dependence on array index j). Maximizing the likelihood over A_f and θ_f leads to

$$A_f = \frac{\left|\sum_{j=1}^{J} \mathbf{d}_{fj}^\dagger \hat{\mathbf{d}}_{fj}(\mathbf{x})\right|}{\sum_{j=1}^{J} \left|\hat{\mathbf{d}}_{fj}(\mathbf{x})\right|^2} , \quad e^{i\theta_f} = \left[\frac{\sum_{j=1}^{J} \hat{\mathbf{d}}_{fj}^\dagger(\mathbf{x})\mathbf{d}_{fj}}{\sum_{j=1}^{J} \mathbf{d}_{fj}^\dagger \hat{\mathbf{d}}_{fj}(\mathbf{x})}\right]^{1/2} \quad (5)$$

for source amplitude and phase, respectively. Substituting back into (2) leads to the ML processor for relative amplitude and phase information known between arrays (termed the *coherent multiple-array processor*, denoted E_{rr})

$$E_{\mathrm{rr}} = \sum_{f=1}^{F} \left\{\sum_{j=1}^{J} \frac{|\mathbf{d}_{fj}|^2}{\sigma_{fj}^2} - \frac{\left|\sum_{j=1}^{J} \frac{\mathbf{d}_{fj}^\dagger \hat{\mathbf{d}}_{fj}(\mathbf{x})}{\sigma_{fj}}\right|^2}{\sum_{j=1}^{J} \left|\hat{\mathbf{d}}_{fj}(\mathbf{x})\right|^2}\right\} . \quad (6)$$

This processor assumes time-synchronized arrays which allows for spatially coherent processing over all arrays; the correlation terms are summed coherently over arrays before normalization (by the squared magnitude of the replica summed over all arrays). Further, it is clear that (6) is equivalent to (at each frequency) concatenating the complex acoustic fields at all arrays into a single supervector and applying the Bartlett processor.

Third, we consider an intermediate case where relative amplitudes are known for all arrays (i.e., relative array calibrations known) but relative phase is not known between

arrays (e.g., arrays are not synchronized with each other in time). The source term is then $S_{fj} = A_f e^{i\theta_{fj}}$ (i.e., amplitude depends on frequency but not on array, while phase depends on both frequency and array), and maximizing the likelihood leads to

$$A_f = \frac{\sum_{j=1}^{J} \left| \mathbf{d}_{fj}^{\dagger} \hat{\mathbf{d}}_{fj}(\mathbf{x}) \right|}{\sum_{j=1}^{J} \left| \hat{\mathbf{d}}_{fj}(\mathbf{x}) \right|^2} \; , \; e^{i\theta_{fj}} = \left[\frac{\hat{\mathbf{d}}_{fj}^{\dagger}(\mathbf{x}) \mathbf{d}_{fj}}{\mathbf{d}_{fj}^{\dagger} \hat{\mathbf{d}}_{fj}(\mathbf{x})} \right]^{1/2} . \quad (7)$$

Substituting back into (2) leads to the processor for relative amplitude and unknown phase information (the *relative-amplitude multiple-array processor*, E_{ru})

$$E_{ru} = \sum_{f=1}^{F} \left\{ \sum_{j=1}^{J} \frac{\left| \mathbf{d}_{fj} \right|^2}{\sigma_{fj}^2} - \frac{\left(\sum_{j=1}^{J} \frac{\left| \mathbf{d}_{fj}^{\dagger} \hat{\mathbf{d}}_{fj}(\mathbf{x}) \right|}{\sigma_{fj}} \right)^2}{\sum_{j=1}^{J} \left| \hat{\mathbf{d}}_{fj}(\mathbf{x}) \right|^2} \right\} . \quad (8)$$

Note that this processor involves incoherent summation of correlations over arrays, but the correlations are summed before normalization by (summed) replica field amplitudes to preserve relative amplitude information in the sum. Hence, with this processor the observed amplitude variations between arrays provide information on source location which is not present in E_{uu} [see (4)]. In many practical cases involving multiple nonsynchronized arrays, array calibrations are known and this new processor can be applied.

A fourth processor for synchronized but noncalibrated arrays can also be considered; however, it does not appear to be possible to derive a closed-form expression for this processor. This processor is considered to be an unusual arrangement of less practical value and is not considered further in this paper.

For comparison with earlier work on MFP, we also consider a processor based on an unweighted, incoherent sum over normalized Bartlett processors (in the following termed the *incoherent array Bartlett prosessor*, denoted E_{BI}) given by

$$E_{BI} = \sum_{f=1}^{F} \sum_{j=1}^{J} \left\{ 1 - \frac{\left| \mathbf{d}_{fj}^{\dagger} \hat{\mathbf{d}}_{fj}(\mathbf{x}) \right|^2}{\left| \mathbf{d}_{fj} \right|^2 \left| \hat{\mathbf{d}}_{fj}(\mathbf{x}) \right|^2} \right\} . \quad (9)$$

This processor is related to the incoherent multiple-array processor E_{uu}, but differs in the weighing factors [in (4)] equal to the data magnitude squared over the noise variance [omitted in (9)].

Table I summarizes appropriate source terms and ML processors for the three cases of practical interest considered above. Note that the approach is general and can be applied to any combination of spectral information, e.g., processors that combine synchronized arrays with nonsynchronized arrays can be derived. The approach does not make assumptions on array geometries and is applicable to any combination of array configurations. Processors that apply ML estimates for unknown error variances can also be derived [19], [21]. ML processors can also be derived assuming knowledge of the source frequency spectrum [19], [20] (i.e., relative source amplitude and/or phase

TABLE I
MAXIMUM-LIKELIHOOD MULTIPLE-ARRAY PROCESSORS AND SOURCE TERMS FOR VARIOUS STATES OF KNOWLEDGE OF RELATIVE AMPLITUDE AND PHASE BETWEEN ARRAYS: r IS RELATIVE KNOWLEDGE; u IS UNKNOWN. SEE TEXT FOR SYMBOL DEFINITIONS

Amplitude/ Phase	Source Term	ML-Processor
u/u	$A_{fj} e^{i\theta_{fj}}$	$E_{uu} = \sum_{f=1}^{F} \sum_{j=1}^{J} \frac{1}{\sigma_{fj}^2} \left\{ \left\| \mathbf{d}_{fj} \right\|^2 - \frac{\left\| \mathbf{d}_{fj}^{\dagger} \hat{\mathbf{d}}_{fj}(\mathbf{x}) \right\|^2}{\left\| \hat{\mathbf{d}}_{fj}(\mathbf{x}) \right\|^2} \right\}$
r/u	$A_f e^{i\theta_{fj}}$	$E_{ru} = \sum_{f=1}^{F} \left\{ \sum_{j=1}^{J} \frac{\left\| \mathbf{d}_{fj} \right\|^2}{\sigma_{fj}^2} - \frac{\left(\sum_{j=1}^{J} \frac{\left\| \mathbf{d}_{fj}^{\dagger} \hat{\mathbf{d}}_{fj}(\mathbf{x}) \right\|}{\sigma_{fj}} \right)^2}{\sum_{j=1}^{J} \left\| \hat{\mathbf{d}}_{fj}(\mathbf{x}) \right\|^2} \right\}$
r/r	$A_f e^{i\theta_f}$	$E_{rr} = \sum_{f=1}^{F} \left\{ \sum_{j=1}^{J} \frac{\left\| \mathbf{d}_{fj} \right\|^2}{\sigma_{fj}^2} - \frac{\left| \sum_{j=1}^{J} \frac{\mathbf{d}_{fj}^{\dagger} \hat{\mathbf{d}}_{fj}(\mathbf{x})}{\sigma_{fj}} \right|^2}{\sum_{j=1}^{J} \left\| \hat{\mathbf{d}}_{fj}(\mathbf{x}) \right\|^2} \right\}$

over frequencies); such processors are not usually applicable to localizing unknown sources and are not considered here.

III. SIMULATION STUDY

The performance of the multiple-array processors derived in this paper is compared by applying Monte Carlo appraisal analysis to a shallow-water test case. This involves applying the processors to a large number of realizations of random source positions/depths and noise, and computing the probability of correct localization defined as the fraction of realizations where the source is localized within an acceptable position and depth interval of the true source location [acceptable (x, y)-position and depth errors are set to 200 and 4 m, respectively, in the examples considered below]. The PCL is a binomial-distributed random variable (localization is either acceptable or not) with a standard deviation estimate given by

$$\sigma = \sqrt{\frac{\text{PCL}(1 - \text{PCL})}{N}} \quad (10)$$

where N is the number of trials.

A. Test Case Description

The test cases involve simulated acoustic data in a 100-m-deep acoustic waveguide. A source at a random depth between 4 and 96 m and random position within a 10-km by 10-km area transmits a signal at frequencies of 200, 300, and 400 Hz. At each frequency, complex Gaussian errors are added to the synthetic data with noise variances set to achieve a given SNR at a specified array; SNRs at the other arrays generally differ due to propagation effects. [SNR is here defined by $\text{SNR} = 10 \log_{10}(\left| \mathbf{d}_{fj} \right|^2 / \left| \mathbf{n}_{fj} \right|^2)$ with $\mathbf{n}_{fj}$ the complex noise
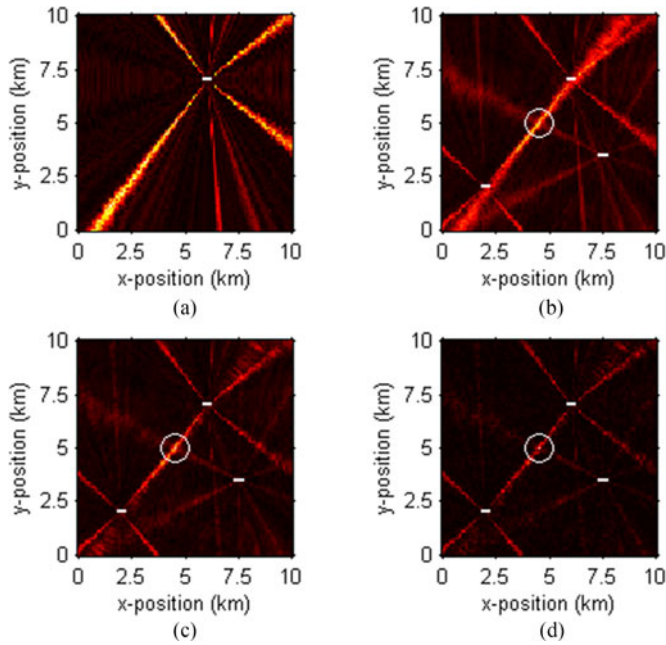
Fig. 1. Two-dimensional horizontal ambiguity surfaces for (a) one HLA processed with E_1, and three HLAs processed with (b) E_{uu}, (c) E_{ru}, and (d) E_{rr}. White circles are centered on the minimum processor value in (b)–(d), and white lines indicate arrays (not to scale). The source is at (x, y) position (4.5, 5) km and depth 20 m. (a) is normalized independently from panels (b)–(d) for display purposes.

Fig. 2. (a) PCL versus SNR for three HLAs processed with E_{rr} (filled circles), E_{ru} (diamonds), E_{uu} (open circles), and E_{BI} (open squares). Vertical lines indicate one standard-deviation error bars. (b) PCL for position-error and (c) PCL for depth-error only; these panels also include PCL versus SNR for one HLA processed with E_1 (triangles).

vector over the array at the fth frequency and jth array.] The environmental model consists of a water column of depth $D = 100$ m and a semi-infinite seabed with sound speed $c_b = 1580$ m/s, density $\rho_b = 1.50$ g/cm^3, and attenuation $\alpha_b = 0.1$ dB/wavelength. The water-column sound-speed profile is defined by sound speeds of 1514 and 1510 m/s at depths of 0 and 100 m, respectively. The 3-D localization search grid covers 0–10-km range in two horizontal directions x and y (grid spacing 100 m) and 4–96 m in depth (grid spacing 2 m). The normal-mode numerical propagation model ORCA [22] is used to compute synthetic data and replica acoustic pressure fields in the frequency domain. Note that the simulated data (and replica fields) are the same for all processors evaluated, but different assumptions on relative array calibration and time synchronization are applied in the processors.

B. Localization With Multiple HLAs

In the first example, data are received at three HLAs on the seafloor. Each array is 128 m long and comprises 24 sensors equally spaced at 5.56-m intervals. The HLAs are located with their centers at (x, y) positions of (6, 7), (2, 2), and (7.5, 3.5) km, respectively, and oriented parallel to the x-axis. Fig. 1 shows 2-D horizontal ambiguity surfaces (cut from the 3-D search grid at the depth of the minimum processor value, which also corresponds to the true source depth) computed for a source at a position of (4.5, 5) km and a depth of 20 m, with noise variances and source strengths set to yield an SNR of 0 dB (at each frequency) at the first array. (The noise variances at the other arrays are set equal to the variances at the first array;
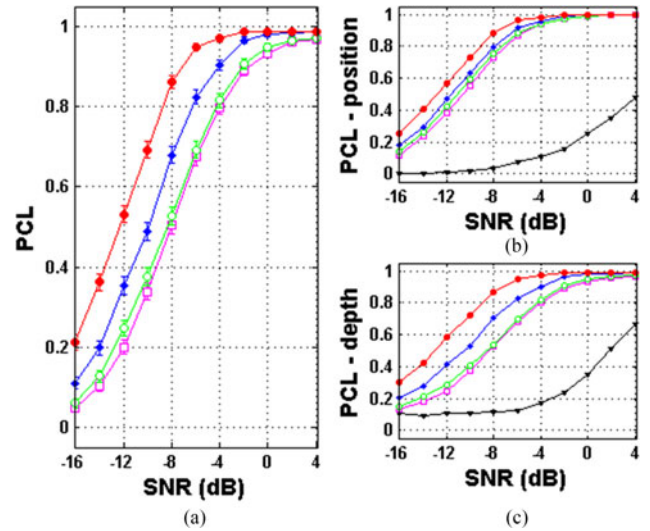
this yielded SNRs of -3 and -4 dB at the second and third arrays, respectively.) Fig. 1(a) shows results for processing of the first array alone with processor E_1 [obtained from processor E_{uu}, in (4), for $J = 1$]. There are multiple directions (akin to grating lobes in conventional beamforming) of low processor values (bright colors) in addition to the direction of the source. These multiple directions can be attributed to insufficient spatial resolution of propagating modes with a relatively sparse horizontal array [23], [24]. Also apparent is the inherent left/right ambiguity of an HLA; for each direction of low processor values there is a mirror direction (about the array length axis) of equal values; hence, there is no unambiguous source location estimate. Fig. 1(b)–(d) shows results for processing of three HLAs with the incoherent multiple-array processor (E_{uu}), the relative-amplitude multiple-array processor (E_{ru}), and the coherent multiple-array processor (E_{rr}), respectively. The minimum processor value (indicated by a white circle) is at the true source position, and there is no ambiguity due to left/right symmetry. Additional secondary minima are located at intersections of directions of low processor values emanating from each array. The relative strength of these secondary minima, as well as the extent of the areas containing the true and secondary minima, progressively decreases [Fig. 1(b)–(d)] as interarray information is added in the processor.

Fig. 2(a) shows processor performance in terms of PCL for SNR varied from -16 to $+4$ dB (in steps of 2 dB) for the three ML processors of Table I, and for the processor E_{BI}. The PCL values are based on simulations for 500 trial source positions and noise realizations. With three HLAs, PCLs of 0.06–0.21 at -16-dB SNR increasing to 0.82–0.97 at -4-dB SNR and above are achieved, depending on the processor. Processing with E_{uu} (open circles) and E_{BI} (open squares) yields comparable results, although the incoherent multiple-array processor E_{uu} is consistently slightly better. Processing with the relative-amplitude
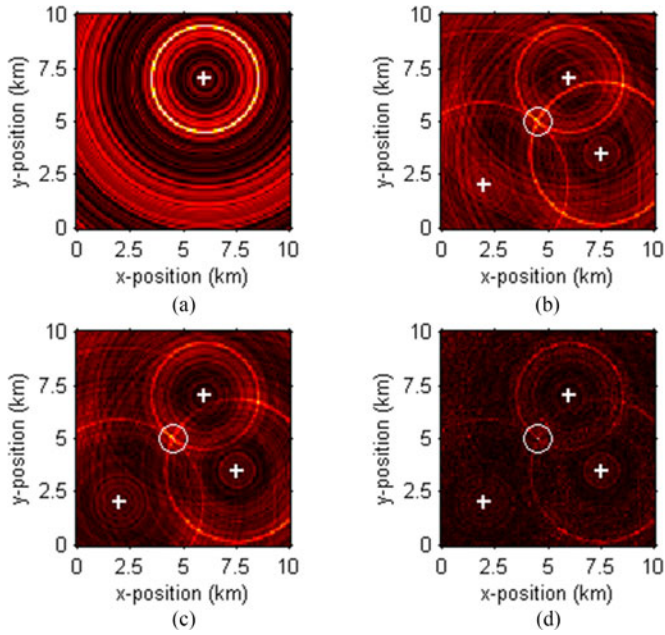
Fig. 3. Two-dimensional horizontal ambiguity surfaces for (a) one VLA processed with E_1, and three VLAs processed with (b) E_{uu}, (c) E_{ru}, and (d) E_{rr}. White circles are centered on the minimum processor value in (b)–(d), and white crosses indicate array locations. The source is at (x, y) position (4.5, 5) km and depth 20 m. (a) is normalized independently from (b)–(d) for display purposes.

Fig. 4. (a) PCL versus SNR for three VLAs processed with E_{rr} (filled circles), E_{ru} (diamonds), E_{uu} (open circles), and E_{BI} (open squares). Vertical lines indicate one standard-deviation error bars. (b) PCL for position error and (c) PCL for depth error only; these panels also include PCL versus SNR for one VLA processed with E_1 (triangles).

processor E_{ru} (diamonds) significantly improves performance over that obtained with E_{BI} and E_{uu} at all SNRs; for example, at -10-dB SNR, PCL increases from 0.34 (for E_{BI}) to 0.49 (for E_{ru}), a 44% improvement. Best overall performance for HLAs in Fig. 2(a) is obtained with the coherent multiple-array processor E_{rr} (filled circles); at -10-dB SNR, PCL increases to 0.69. To further investigate the results, Fig. 2(b) and (c) shows PCL separated for horizontal position error and for depth error individually (note that an estimate can be acceptable in position and not acceptable in depth, and *vice versa*). In these figures, results for processing with a single HLA (the first array) with E_1 are also included (triangles). With a single HLA, the position-error PCL and the depth-error PCL are overall low but increase with SNR. The improved performance with E_{ru} over E_{uu} (and E_{BI}) can be attributed to improved position-error PCL and much improved depth-error PCL. The range/depth localization ability of an HLA is reliant on accurate modeling of amplitude variation with range along the array [24], thus the use of relative amplitude information between arrays can explain the increase in performance with E_{ru} over E_{uu} (and E_{BI}) with multiple HLAs.

C. Localization With Multiple VLAs

In the second example, data are received at three VLAs, with each array comprising 24 sensors equally spaced at 4-m intervals from 4- to 96-m depth. The VLAs are located at (x, y) positions of (6, 7), (2, 2), and (7.5, 3.5) km, respectively. Fig. 3 shows 2-D horizontal ambiguity surfaces computed for a source at position (4.5, 5) km and depth 20 m with noise variances and source strengths set to yield an SNR of 0 dB at the first array (SNRs of -3 and -4 dB at the second and third arrays,
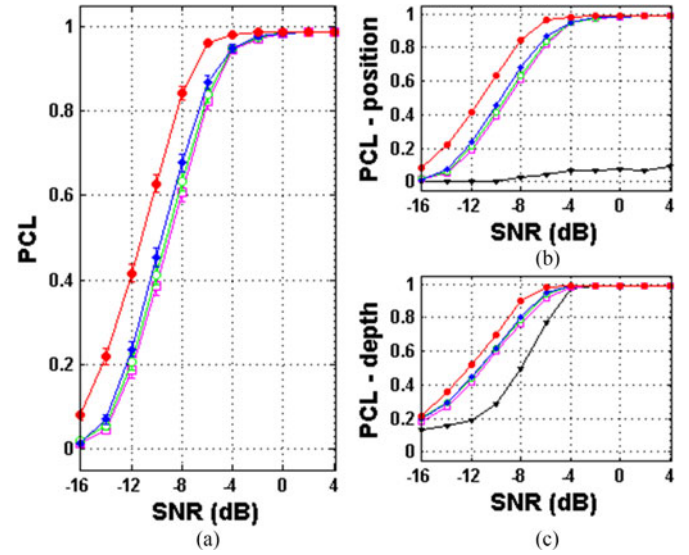
respectively). Fig. 3(a) shows results for processing data from the first array alone with processor E_1. There is a circle of low processor values (bright colors) at the correct source-to-array range; this shows the ability of a VLA for range (and depth) localization but no direction discrimination and hence no 3-D localization capability. Fig. 3(b)–(d) shows results for processing data from three VLAs with E_{uu}, E_{ru}, and E_{rr}, respectively. For all processors, the minimum occurs at the true source position, demonstrating the ability for 3-D localization (in horizontal position and depth) with multiple VLAs. For all cases, the minimum is at the intersection of concentric circles around each of the three arrays; additional secondary minima are located along these circles and at their points of intersection. The relative difference between the minimum processor value and the secondary minima progressively increases [Fig. 3(b)–(d)] as interarray information is added in the processor.

Fig. 4 shows processor performance in terms of PCL for SNR varied from -16 to $+4$ dB for the three ML multiple-array processors, for the processor E_{BI}, and for processing the first VLA alone. With three VLAs, PCLs of 0.02–0.08 at -16-dB SNR increasing to 0.94–0.98 at -4-dB SNR and above are achieved, depending on the processor. Processing with E_{uu} and E_{ru} yields comparable results, although the relative-amplitude processor E_{ru} is consistently slightly better; for example, at -10-dB SNR, the PCL is 0.41 and 0.45, respectively. This is in contrast to the HLA case (Fig. 2), where performance with E_{ru} was significantly better than E_{uu}. Both E_{uu} and E_{ru} are consistently better than the Bartlett processor E_{BI}; for example, at -10-dB SNR, the PCL is 0.39 with E_{BI}. Processing with the coherent processor E_{rr} improves performance notably over that obtained with all other processors; for example, at -10-dB SNR, PCL increases to 0.63. Fig. 4(b) and (c) shows that with
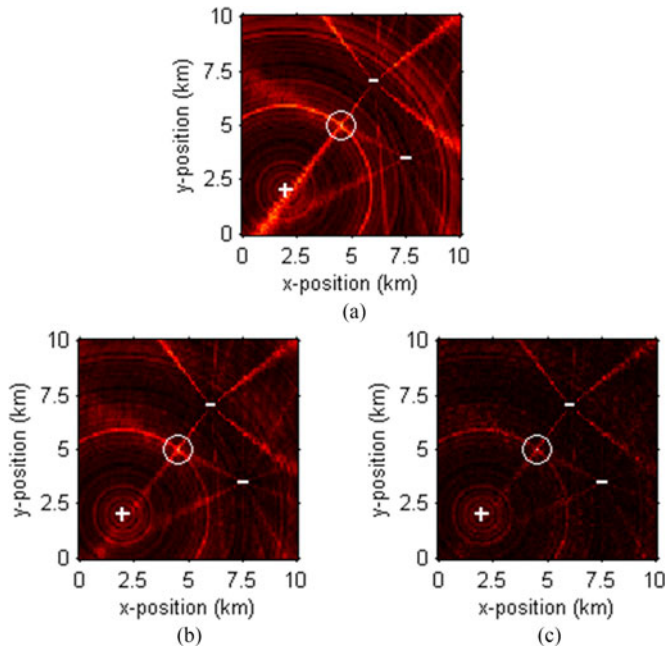
Fig. 5. Two-dimensional horizontal ambiguity surfaces for two HLAs and one VLA processed with (a) E_{uu}, (b) E_{ru}, and (c) E_{rr}. White circles are centered on the minimum processor value in (a)–(c), and white symbols indicate arrays (not to scale). The source is at (x,y) position (4.5,5) km and depth 20 m.

Fig. 6. (a) PCL versus SNR for two HLAs and one VLA processed with E_{rr} (filled circles), E_{ru} (diamonds), E_{uu} (open circles), and E_{BI} (open squares). Vertical lines indicate one standard-deviation error bars. (b) PCL for position error and (c) PCL for depth error only.

a single VLA, the position-error PCL is consistently low while the depth-error PCL increases with SNR to near 1.0 at 0-dB SNR; this reflects the depth localization ability but poor position localization ability due to circular symmetry of a VLA. (The nonzero position-error PCL at higher SNR, e.g., $\mathrm{PCL} = 0.07$ at 4-dB SNR, is due to improved range localization with SNR and hence an improved chance of generating a position along the ambiguity circle that is also within the acceptable position error.) With multiple VLAs, position localization ability is acquired, although the position-error PCL is consistently lower than the depth-error PCL. Fig. 4(b) and (c) also indicates that the improved performance with E_{rr} over the other processors is primarily due to improved position-error PCL. This can be understood from the fact that the range/depth localization ability of a VLA is reliant on accurate modeling of a rapidly varying phase with depth over the array; exploiting phase information between multiple VLAs improves the accuracy of this modeling. From Fig. 4(c), also note that the depth-error PCL is better than that obtained for HLAs [Fig. 2(c)]. Finally, comparing results for three VLAs [Fig. 4(a)] with those obtained for three HLAs [Fig. 2(a)], at −16-dB SNR performance is better for HLAs than VLAs (all processors); at higher SNRs E_{uu} performance is better for VLAs while E_{rr} performance is better for HLAs and E_{ru} performance is mixed.

D. Localization With HLAs and VLAs

In the third example, the array configuration in the first example (Section III-B) is changed such that the HLA at position (2, 2) km is replaced with a VLA [the two HLAs at positions (6, 7) and (7.5, 3.5) km are retained]. Fig. 5 shows horizon-
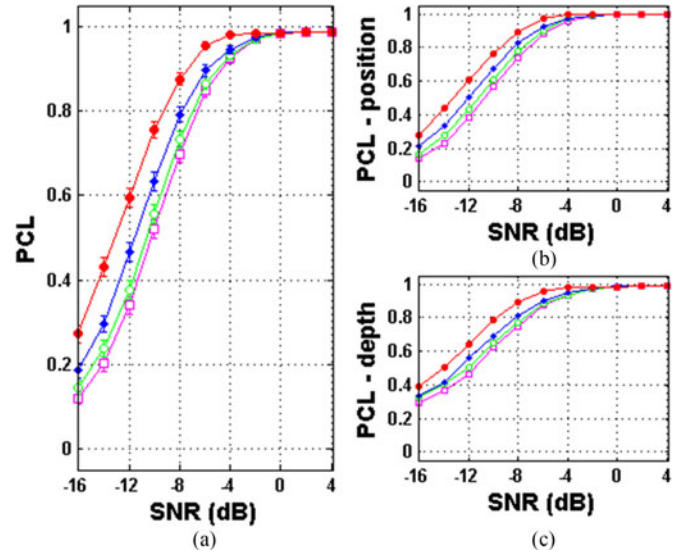
tal ambiguity surfaces computed for a source at position (4.5, 5) km and depth 20 m with noise variances and source strengths set to yield an SNR of 0 dB at the HLA in position (6, 7) km (SNRs of 0 and −4 dB at the VLA and second HLA, respectively). Fig. 5(a)–(c) shows results for processing of the three arrays with E_{uu}, E_{ru}, and E_{rr}, respectively. The minimum processor value is at the true source position, at the intersection of a circle around the VLA and beams of low processor values emanating from each of the two HLAs. Additional secondary minima are located along the circle around the VLA, as well as along the HLA beams and at intersections of HLA beams.

Fig. 6(a) shows processor performance in terms of PCL for SNR varied from −16 to +4 dB. Overall, these results are the best of the three examples examined, for all processors. For example, at −10-dB SNR, PCL is 0.52 with E_{BI} (0.39 for three VLAs and 0.34 for three HLAs), increasing to 0.63 with E_{ru} (0.45 for three VLAs and 0.49 for three HLAs), and to 0.76 with E_{rr} (0.63 for three VLAs and 0.69 for three HLAs). In terms of comparison between processors, Fig. 6(a) shows that the consistently best results are obtained by the coherent processor E_{rr} followed by E_{ru}, E_{uu}, and E_{BI}. Examining Fig. 6(b) and (c), the position-error PCL is comparable to that obtained with three HLAs [Fig. 2(b)], while the depth-error PCL is improved over that obtained with three HLAs [Fig. 2(c)] and comparable to that obtained with three VLAs [Fig. 4(c)]. This indicates that the replacement of one HLA with a VLA improved depth localization and contributed to the overall best performance of the three array configurations studied.

E. Multiple Frequencies

This section considers processor performance as a function of the number of frequencies applied in processing. Note that this does not assume knowledge of the source frequency spectrum,
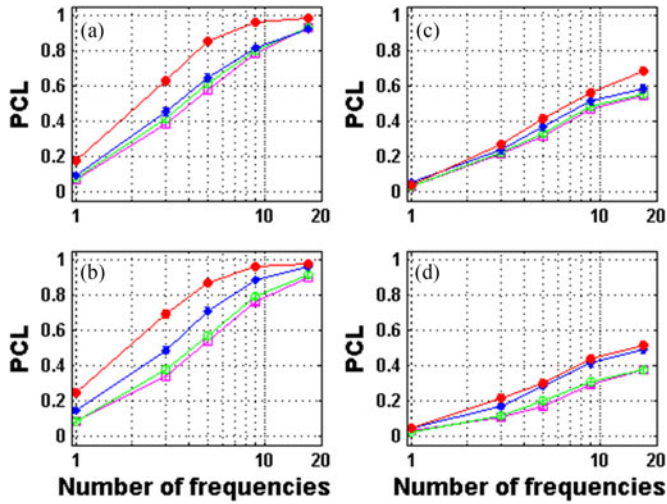
Fig. 7. PCL at -10-dB SNR as a function of the number of frequencies in (a) and (b) true environment, and (c) and (d) mismatched environments. The array configurations are: three VLAs (upper row) and three HLAs (lower row). The processors are E_{rr} (filled circles), E_{ru} (diamonds), E_{uu} (open circles), and E_{BI} (open squares). Vertical lines indicate one standard-deviation error bars.

and, for simplicity, the SNR is taken to be constant over frequency. Fig. 7 (left panels) shows PCL for processing of three arrays with the number of frequencies (equally spaced from 200 to 400 Hz) varied from 1 to 17, at -10-dB SNR, for the cases of three VLAs [Fig. 7(a)] and three HLAs [Fig. 7(b)]. In general, performance increases with the number of frequencies, with the rate of improvement decreasing as the number of frequencies increases. This is in accordance with previous results for a single VLA [20]. Increasing the number of frequencies does not significantly alter the relative performance of the four processors (from that observed in Sections III-B and III-C) for either of the array configurations studied.

F. Environmental Mismatch

A well-known problem in MFP is environmental mismatch, where uncertainty in environmental parameters can degrade processor performance due to modeling errors in the replica fields [18], [25], [26]. To investigate such effects, for each random source position considered in the Monte Carlo analysis, a random realization of each of the water depth (D) and seabed geoacoustic model parameters (c_b, ρ_b, α_b) is drawn uniformly at random within ± 2 m, ± 10 m/s, ± 0.14 g/cm^3, and ± 0.08 dB/wavelength, respectively, of their true values, and used in computing the replica fields. Mismatch can also be due to uncertainty in sound speed in the water column; for the shallow-water, range-independent sound-speed profile considered here, effects of uncertainty in sound speed were found to be much less than effects due to uncertainty in seabed parameters and water depth.

Fig. 7 (right panels) shows PCL for processing of three arrays in mismatched environments with the number of frequencies varied from 1 to 17, at -10-dB SNR, for three VLAs [Fig. 7(c)] and three HLAs [Fig. 7(d)]. In general, processor performance is significantly degraded over performance in the

exact environment (corresponding left panels of Fig. 7), for all processors and all array configurations. For example, with three VLAs and three frequencies, the PCL for E_{rr} decreases from 0.63 [Fig. 7(a)] to 0.27 [Fig. 7(c)]; with three HLAs and three frequencies, the PCL for E_{rr} decreases from 0.69 [Fig. 7(b)] to 0.22 [Fig. 7(d)]. Significant degradations can be seen also for the other processors.

It is also observed that the improved performance obtained with the coherent processor E_{rr} over the relative-amplitude processor E_{ru} (and the incoherent processor E_{uu}) in the exact environment is diminished or lost in the presence of environmental mismatch. For example, with three VLAs and five frequencies in mismatched environments [Fig. 7(c)], E_{rr} yields an improvement over E_{ru} (PCLs of 0.42 and 0.37, respectively); with three HLAs and five frequencies [Fig. 7(d)] the improvement with E_{rr} over E_{ru} is less (PCLs of 0.30 and 0.29, respectively). Thus, the coherent processor has a stronger sensitivity to environmental mismatch than the relative-amplitude and incoherent processors; this is likely because mismatch affects the phase of the modeled fields more strongly than the amplitude. Hence, using information on the relative phase between arrays is less advantageous in the presence of environmental mismatch. Significantly, the relative-amplitude processor E_{ru} remains superior to the incoherent processor E_{uu} in all mismatch cases in Fig. 7.

Next, we compare the performance with few frequencies in the exact environment (left panels of Fig. 7) with the performance with many frequencies in mismatched environments (right panels of Fig. 7). For example, for three VLAs and three frequencies, with E_{rr}, the PCL decreases from 0.63 (exact) to 0.27 (mismatched environments); however, with 17 frequencies in mismatched environments, the performance improves to PCL $= 0.69$ (better than for three frequencies and no mismatch). For three HLAs and three frequencies, with E_{rr}, the PCL decreases from 0.69 (exact) to 0.22 (mismatched environments); in mismatched environments, PCL $= 0.52$ is obtained with 17 frequencies. Thus, it appears that degradation due to environmental mismatch can in part be mitigated by applying additional frequencies in processing, at least for the examples considered here. (Similar observations have been made for simulated scenarios with a single VLA [27].)

G. Array Mismatch

Mismatch can also be due to system factors that include errors in relative array calibration and errors in time synchronization between two or more arrays. To investigate such effects, for each random source position considered in the Monte Carlo analysis, a constant calibration error of ± 3 dB (i.e., an increase or reduction by 30% in pressure-field magnitude), or a constant time offset of ± 0.5 ms is applied to the replica fields (positive error for the second, and negative for the third array, respectively).

Fig. 8(a) and (b) shows the PCL as a function of the number of frequencies at -10-dB SNR with system mismatch due to calibration errors, for three VLAs [Fig. 8(a)] and three HLAs [Fig. 8(b)]. The incoherent processors (E_{uu} and E_{BI}) do not assume relative calibration between arrays and hence are insensitive to these errors. The effect of a ± 3-dB array calibration
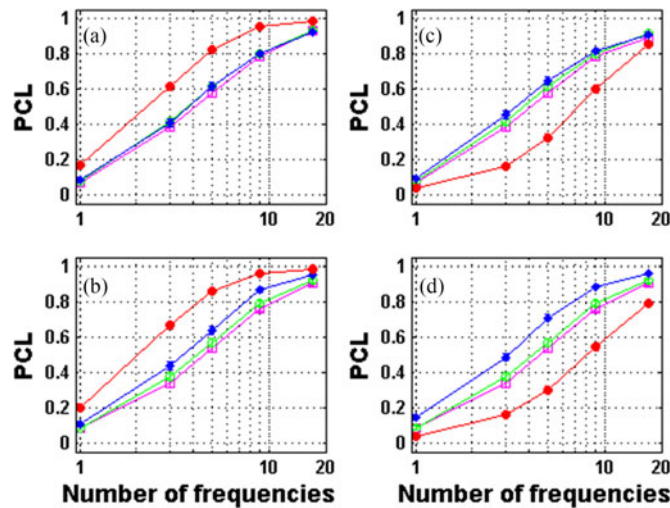
Fig. 8. PCL at -10-dB SNR as a function of the number of frequencies with array mismatch consisting of (a) and (b) 3-dB calibration errors, and (c) and (d) 0.5-ms time-synchronization errors. The array configurations are three VLAs (upper row) and three HLAs (lower row). The processors are E_{rr} (filled circles), E_{ru} (diamonds), E_{uu} (open circles), and E_{BI} (open squares). Vertical lines indicate one standard-deviation error bars.

error on processors E_{ru} and E_{rr} is relatively small. For example, with E_{ru} and three frequencies, the PCL with three VLAs is reduced from 0.45 [Fig. 7(a)] to 0.41 [Fig. 8(a)], with three HLAs from 0.49 [Fig. 7(b)] to 0.44 [Fig. 8(b)]; with E_{rr}, the reductions are smaller. With three HLAs, the performance with E_{ru} is significantly better than E_{uu} and E_{BI}, even in the presence of calibration errors.

Fig. 8(c) and (d) shows the PCL as a function of the number of frequencies at -10-dB SNR with system mismatch due to time-synchronization errors, for three VLAs [Fig. 8(c)] and three HLAs [Fig. 8(d)]. The incoherent processors and processor E_{ru} do not assume time synchronization between arrays and are insensitive to these errors. The effect on processor E_{rr} of array mismatch due to a ± 0.5-ms time offset can be large. For example, with five frequencies the PCL with three VLAs is reduced from 0.85 [Fig. 7(a)] to 0.33 [Fig. 8(c)]; with three HLAs, the PCL is reduced from 0.87 [Fig. 7(b)] to 0.30 [Fig. 8(d)]. In the presence of time-synchronization errors, processor E_{ru} provides best results. These examples indicate that in the presence of array mismatch, processor E_{ru} may be a better choice than processor E_{rr}, even if array synchronization is known.

IV. SUMMARY AND DISCUSSION

This paper developed and examined ML matched-field processors for source localization that optimally combine spectral information between multiple arrays. Three processors that consider various states of relative information applicable to calibrated or uncalibrated and/or time-synchronized or nonsynchronized arrays were considered. The approach is general and can be applied to any combination of information for the component arrays; e.g., processors that combine synchronized arrays with nonsynchronized arrays can be derived. The approach makes no assumptions on array geometries and is applicable to arbitrary array and sensor configurations.

Simulation examples with multiple arrays in a range-independent shallow-water scenario demonstrated that including relative array information consistently improved localization performance. Localization performance, quantified as the probability of correct localization, was examined as a function of SNR and the number of frequencies using Monte Carlo analysis. The examples showed that with multiple vertical and/or horizontal line arrays a significant improvement in performance is obtained with the coherent multiple-array processor, where both relative phase and amplitude information are included (i.e., for time-synchronized and calibrated arrays). With multiple HLAs, improvement in performance is also obtained with the relative-amplitude multiple-array processor, when only relative amplitude information is included (i.e., with calibrated but nonsynchronized arrays). For multiple VLAs, relative amplitude information alone provided a smaller improvement in performance. In terms of the array configurations, best overall results (for all processors) were obtained combining VLAs and HLAs; this combines the good depth-localization capability of a VLA with good position-localization capability of HLAs.

In the presence of mismatch, localization performance is degraded overall compared to the performance obtained in an exactly known scenario. In general, such degradation can in part be mitigated by applying additional frequencies in processing. In mismatched environments, performance degraded such that relative phase information (i.e., for time-synchronized arrays) yields little or no improvement over that obtained without such information (i.e., for nonsynchronized arrays). However, including relative calibration information (in the relative-amplitude processor) improved localization performance in mismatched environments over that obtained with the incoherent processors. In the presence of array mismatch due to errors in time synchronization, the coherent processor (which assumes synchronized arrays) can be severely degraded, such that the relative-amplitude processor provides best results. The effect of errors in relative array calibration is, on the other hand, relatively small. This indicates that in the presence of array mismatch, the relative-amplitude processor may be a better choice than the coherent processor, even if array synchronization is known. An important overall result of this paper is that when relative calibration information is available for multiple arrays (commonly the case, since individual arrays must be calibrated to apply MFP), the new relative-amplitude processor consistently outperforms standard MFP processors which neglect received amplitude information between arrays.

Finally, two other possible sources of error should be discussed, although they are not examined specifically in this paper. A potential error for the relative-amplitude and coherent multiple-array processors could arise for acoustic sources which are not reasonably omnidirectional. At the relatively low frequencies considered here source directionality is generally low; however, for acoustic sources that are strongly directional, these two processors could be significantly degraded. The second is the effect of random spatial and temporal fluctuations of the ocean on acoustic propagation [28], which degrades

the signal coherence between spatially separated arrays (due to stochastic effects along the different source-to-array propagation paths). The incoherent multiple-array processor should not be degraded by random medium effects, as it is based on unknown source signal amplitude and phase spectra for each array (which also accounts for different source-to-array propagation effects). Conversely, the coherent multiple-array processor could be significantly degraded by random effects (for large array separations), as it assumes a coherent signal is maintained along different propagation paths. However, the new relative-amplitude multiple-array processor should be more robust to random propagation as it assumes the same signal amplitude spectrum along different propagation paths, but makes no assumptions about signal-phase coherence (which is likely affected more strongly). Although random medium effects have not been investigated here, we note that simulation studies of environmental and array mismatch showed much smaller degradation for the relative-amplitude multiple-array processor than for the coherent processor.

REFERENCES

[1] E. Sullivan, Z.-H. Michalopoulou, and C. Yardim, "Model-based ocean acoustic signal processing," *Acoust. Today*, vol. 7, pp. 8–16, 2011.

[2] A. B. Baggeroer, W. A. Kuperman, and P. N. Mikhalevsky, "An overview of matched field methods in ocean acoustics," *IEEE J. Ocean. Eng.*, vol. 18, pp. 401–424, 1993.

[3] N. O. Booth, *et al.*, "Source localization with broad-band matched-field processing in shallow water," *IEEE J. Ocean. Eng.*, vol. 21, no. 4, pp. 400–411, 1996.

[4] S. L. Tantum and L. W. Nolte, "Tracking and localizing a moving source in an uncertain shallow water environment," *J. Acoust. Soc. Amer.*, vol. 103, pp. 362–373, 1998.

[5] L. M. Zurk, N. Lee, and J. Ward, "Source motion mitigation for adaptive matched field processing," *J. Acoust. Soc. Amer.*, vol. 113, pp. 2719–2731, 2003.

[6] T. B. Neilsen, "Localization of multiple acoustic sources in the shallow ocean," *J. Acoust. Soc. Amer.*, vol. 118, pp. 2944–2953, 2005.

[7] C. Debever and W. A. Kuperman, "Robust matched-field processing using a coherent broadband white noise constraint processor," *J. Acoust. Soc. Amer.*, vol. 122, pp. 1979–1986, 2007.

[8] P. A. Forero and P. A. Baxley, "Shallow-water sparsity-cognizant source-location mapping," *J. Acoust. Soc. Amer.*, vol. 135, pp. 3483–3501, 2014.

[9] J. Gebbie, M. Siderius, and J. S. Allen III, "A two-hydrophone range and bearing localization algorithm with performance analysis," *J. Acoust. Soc. Amer.*, vol. 137, pp. 1586–1597, 2015.

[10] A. M. Thode, G. L. D'Spain, and W. A. Kuperman, "Matched-field processing, geoacoustic inversion, and source signature recovery of blue whale vocalizations," *J. Acoust. Soc. Amer.*, vol. 107, pp. 1286–1300, 2000.

[11] R. Aubauer, M. O. Lammers, and W. L. Au, "One-hydrophone method of estimating distance and depth of phonating dolphins in shallow water," *J. Acoust. Soc. Amer.*, vol. 107, pp. 2744–2749, 2000.

[12] C. O. Tiemann, M. B. Porter, and L. N. Frazer, "Localization of marine mammals near Hawaii using an acoustic propagation model," *J. Acoust. Soc. Amer.*, vol. 115, pp. 2834–2843, 2004.

[13] A. Thode, "Tracking sperm whale (*Physeter microcephalus*) dive profiles using a towed passive acoustic array," *J. Acoust. Soc. Amer.*, vol. 116, pp. 245–253, 2004.

[14] C. O. Tiemann, A. M. Thode, J. Straley, V. O'Connell, and K. Folkert, "Three-dimensional localization of sperm whales using a single hydrophone," *J. Acoust. Soc. Amer.*, vol. 120, pp. 2355–2365, 2006.

[15] E.-M. Nosal and L. N. Frazer, "Modified pair-wise spectrogram processing for localization of unknown broadband sources," *IEEE J. Ocean. Eng.*, vol. 32, no. 3, pp. 721–728, 2007.

[16] S. H. Abadi, A. M. Thode, S. B. Blackwell, and D. R. Dowling, "Ranging bowhead whale calls in a shallow-water dispersive waveguide," *J. Acoust. Soc. Amer.*, vol. 136, pp. 130–144, 2014.

[17] D. H. Johnson and D. E. Dudgeon, *Array Signal Processing: Concepts and Techniques*. Englewood Cliffs, NJ, USA:Prentice-Hall, pp. 147–151, 1993.

[18] D. R. Del Balzo, C. Feuillade, and M. R. Rowe, "Effects of water-depth mismatch on matched-field localization in shallow water," *J. Acoust. Soc. Amer.*, vol. 83, pp. 2180–2185, 1988.

[19] C. F. Mecklenbräuker and P. Gerstoft, "Objective functions for ocean acoustic inversion derived by likelihood methods," *J. Comput. Acoust.*, vol. 8, pp. 259–270, 2000.

[20] S. E. Dosso and M. J. Wilmut, "Maximum-likelihood and other processors for incoherent and coherent matched-field localization," *J. Acoust. Soc. Amer.*, vol. 132, pp. 2273–2285, 2012.

[21] S. E. Dosso and M. J. Wilmut, "Estimating data uncertainty in matched-field geoacoustic inversion," *IEEE J. Ocean. Eng.*, vol. 31, pp. 470–479, 2006.

[22] E. K. Westwood, C. T. Tindle, and N. R. Chapman, "A normal mode model for acousto-elastic ocean environments," *J. Acoust. Soc. Amer.*, vol. 100, pp. 3631–3645, 1996.

[23] C. W. Bogart and T. C. Yang, "Source localization with horizontal arrays in shallow water: Spatial sampling and effective aperture," *J. Acoust. Soc. Amer.*, vol. 96, pp. 1677–1686, 1994.

[24] S. L. Tantum and L. W. Nolte, "On array design for matched-field processing," *J. Acoust. Soc. Amer.*, vol. 107, pp. 2101–2111, 2000.

[25] A. M. Richardson and L. W. Nolte, "*A posteriori* source localization in an uncertain sound speed, deep ocean environment," *J. Acoust. Soc. Amer.*, vol. 89, pp. 2280–2284, 1991.

[26] M. D. Collins and W. A. Kuperman, "Focalization: Environmental focusing and source localization," *J. Acoust. Soc. Amer.*, vol. 90, pp. 1410–1422, 1991.

[27] S. E. Dosso, J. Dettmer, and M. J. Wilmut, "Efficient localization and spectral estimation of an unknown number of ocean acoustic sources using a graphics processing unit," *J. Acoust. Soc. Amer.*, vol. 138, pp. 2945–2956, 2015.

[28] W. Xu, A. B. Baggeroer, and H. Schmidt, "Performance analysis for matched-field source localization: Simulations and experimental results," *IEEE J. Ocean. Eng.*, vol. 31, pp. 325–344, 2006.

Dag Tollefsen received the Cand. Scient. (M.Sc.) degree in physics from the University of Oslo, Oslo, Norway, in 1988 and the Ph.D. degree from the School of Earth and Ocean Sciences, University of Victoria, Victoria, BC, Canada, in 2010.

Since 1990, he has been with the Norwegian Defence Research Establishment (FFI), Horten, Norway. His current research interests include geoacoustic inversion of experimental data, and Arctic ambient noise.

Dr. Tollefsen is a Member of the Acoustical Society of America.

Stan E. Dosso received the B.Sc. degree in physics and applied mathematics and the M.Sc. degree in physics from the University of Victoria, Victoria, BC, Canada, in 1982 and 1985, respectively, and the Ph.D. degree in geophysics from the University of British Columbia, Vancouver, BC, Canada, in 1990.

From 1990 to 1995, he worked in ocean physics (Arctic acoustics) at the Defence Research Establishment Pacific, Victoria, BC, Canada. In 1995, he was appointed to an Ocean Acoustics Research Chair in the School of Earth and Ocean Sciences, University of Victoria, where he is currently a Professor and Director of the School. His research interests involve inverse problems in ocean acoustics and geophysics.

Dr. Dosso is a Fellow of the Acoustical Society of America and a member of the Canadian Acoustical Association (President 2003–2007) and the American Geophysical Union.